Li on a Ch Divacancy Self-Healed Graphane: A First -Principles Study

Refilwe Edwin Mapasha * , Sentserere Phodisho Kgalema , Hezekia Mapingire , Emmanuel Igumbor

Posted Date: 22 November 2023

doi: 10.20944/preprints202311.1395.v1

Keywords: Graphane; divacancy; lithiation; density functional theory; charge doping; conductivity

Article

Li on a CH Divacancy Self-Healed Graphane: A First-Principles Study

R. E. Mapasha [1,*], S. P. Kgalema [1], H. Mapingire [1] and E. Igumbor [2]

[1] Department of Physics, University of Pretoria, Hatfield campus, Pretoria 0002, RSA
[2] Department of Mechanical Engineering Science, University of Johannesburg, Johannesburg, South Africa
* Correspondence: edwin.mapasha@up.ac.za

Abstract: The possibility of using graphane monolayer crystals as the electrode material is becoming popular. Graphane is stable at room temperature and has large surface area, but its chemical inertness hinders its direct interactions with Li ions. In this study, we performed density functional theory calculations to study the energetic stability, structural and electronic properties of Li on graphane with various CH divacancy configurations (v_{12}, v_{13} and v_{14}). The results show that adsorption of Li atom reduces the formation energy of the CH divacancy configurations. The Li-v_{12} is most stable with the highest binding energy of 3.25 eV/Li and relaxes to in-plane with other C atoms. Altering the Li charge state to have Li^{-1}-v_{12} or Li^{+1}-v_{12} affects the energetic stability and electronic characters of Li-v_{12}. The Li^{-1}-v_{12} (Li^{+1}-v_{12}) enhances (reduces) the binding force between Li and v_{12} configuration, and furthermore it improves (deteriorates) the conductivity of the structure. Further investigation of graphane with vacancies is encouraged due to these intriguing observations, as it holds promise for potential utilization as an electrode material.

Keywords: graphane; divacancy; lithiation; density functional theory; charge doping; conductivity

1. Introduction

Lithium-ion batteries (LIBs) have been widely used as power sources for most of electronic devices[1]. The LIBs are known to be non-toxic, have long discharging rate, have high energy density etc[1–3]. The most used electrode in LIBs is graphite [1]. Nevertheless, many properties, such as the specific capacity, are unlikely to meet the increasing future demand for high energy. The search for alternative electrode materials with distinct properties from graphite is rapidly intensifying [4–6]. The two-dimensional (2D) materials are emerging as promising candidates to address future energy demands due to their high electrical conductivity, reduced dimensionality, high thermodynamic stability, large surface area etc., distinguishing them from their bulk counterpart [7–9]. These properties make 2D materials well suited to accommodate a greater number of Li atoms, among other advantages.

Graphane [10] monolayer material falls under materials belonging to the graphene derivatives were each carbon is bonded to hydrogen atom in an alternating pattern. The realization of graphane was first reported by Sluiter et al. [11], based on the density functional theory (DFT). Graphane was later synthesized [12,13] by applying hydrogen plasma to graphene monolayer samples. The graphane samples were found to be stable at room temperatures [12]. Each carbon atom's bonding network takes on the form of sp^3 hybridization due to the presence of hydrogen atoms [13].

Experimental studies report that graphane has insulating characters [12]. This was supported by the theoretical studies which predicted the energy band gap of 3.50 eV (standard DFT) [10], 5.40 eV (GW)[14], 4.21 eV (HSE06)[15]. Graphane has a large surface area, high volumetric capacity, non-toxic samples [13,16,17]. These indicators suggest that a graphane monolayer could find utility in a range of technological application. The focus of this work is on the mechanisms of enchoring the Li ions on the graphane monolayer for electrode exploitation. Theoretically, an inertness [13,16,17] (under ambient conditions) of C atoms conjugating graphane monolayer due to the sp^3 bonding network could physisorb instead of chermisorbing Li ions, which will be a setback for encoring Li atoms. Watcharinyanon et al. [18] studied intercalation of Li ions on graphane using experimental

 doi:10.20944/preprints202311.1395.v1

techniques. They reported that instead of bonding with the substrate Li atoms form islands among themselves. The DFT studies by Yang et al. [19] revealed that Li ions are screened by H atoms, as such no chemisorption takes place.

The modification of graphane monolayer for possibility of enhancing Li interaction is necessary. Several methods are known for introducing reactive sites on graphane, potentially enhancing its interaction with Li ions. These methods include structural modification like creating vacancies, doping, strain application, among others [13,16,17,20]. Creation of vacancies in graphane can primarily be in different forms: hydrogen (H) vacancy, carbon (C) vacancy, carbon-hydrogen (CH) vacancy.The creation of multiple vacancies is also possible in graphane monolayer. H divacancy, trivacancy and CH divacancy, trivacancy have been created in graphane monolayer. These vacancies can be created by applying high or low ions bombardment, and they can also occur during synthetic processes [13,16, 17,20]. Numerous properties of these mentioned vacancies have been examined, ranging from their energetic stabilities to their magnetic properties [13,16,17,20–24]. With the exception of the divacancy structure, all other types of vacancies introduce mid-gap states within the band gap and exhibit magnetic properties.

The structural and electronic behavior of CH divacancies in graphane have been studied using DFT [24]. The structural reconstruction of the two adjacent vacancies has been reported, which break the hexagonal symmetry and translates into the new 5-8-5 defect structure that is thermodynamically stable. Graphane with 5-8-5 defect structure is characterized as a wide band gap material [24]. Considering the potential of utilizing graphane with this defect structure as an electrode holds merit. Notably, the adsorption of Li ions onto the graphane with 5-8-5 defect structure remains unexplored. A comprehensive understanding of how Li anchors at different charge states on graphane is imperative. This helps to understand the energetic and electronic behavior of Li during charging and discharging. This study intends to understand the energetic stabilities (formation energy and binding energy), structural properties (bondlength) and electronic properties (density of states) of Li on the graphane with 5-8-5 defect structure at different Li charge states (+1 or -1). This study relies on a spin-polarized density functional theory approach, and the outcomes will serve as a reference for the experimentalists to corroborate their findings during practical synthesis and characterization processes.

This manuscript is arranged as follows: the computational details and equations for calculating formation and binding energies are presented in section 2. The results of Li on graphane monolayer with vacancies are summarized in section 3. Section 4 concludes the results.

2. Computational Details

All the spin polarized calculations in this study have been performed using hybrid density functional theory (DFT) approach implemented within the Vienna *ab initio* simulation package (VASP) code [25]. The chosen hybrid exchange correlation functional is the Heyd, Scuseria, and Ernzerhof (HSE06) [26], which the PBE functional is mixed with the non-local Fock. The Fock mixing parameter used is 0.25 which it is known to give the correct band gap of 2D materials. In this study it was selected with the intention of enhancing the magnitude of the band gap and providing a more accurate description of the positions of electronic states induced by defects within the band gap. For the description of pseudopotentials, the projector augmented wave (PAW) methods [27] with C atoms represented as $2s^2 2p^2$, H atoms represented by $1s^1$ and Li adatom represented as $2s^1$ valence electrons.

The kinetic energy cut-off of 500 eV was used for the expansion of the plane wavefunctions. For sampling the Brillouin zone of graphane monolayer, the $6\times6\times1$ k-mesh grid was used, employing the Monkhorst-Pack scheme [28] method. This k-mesh grid is doubled during the density of states calculations. The atomic positions were allowed to relaxe until their residual forces are less than 0.01 eVÅ^{-1} utilizing the Hellman-Feynman theorem. The total energies of the structures were allowed to converge to within 10^{-7} eV during the self-consistent field calculations of each relaxation. The 9×9 supercell of graphane was used for all our calculations. This supercell size was chosen to ensure that the divacancy interaction between the cell images along the x and y direction is minimal. The

Preprints (www.preprints.org) | NOT PEER-REVIEWED | Posted: 22 November 2023 doi:10.20944/preprints202311.1395.v1

separation spacing between the layers was set to the converged 20 Å , to avoid unwanted interactions due to periodic images.

To study the energetic stability of Li on a graphane with various CH divacancy configurations (v_{12}, v_{13} and v_{14}), their formation energies were calculated employing the Zhang-Northrup expression [29] below:

$$E_f(CH) = E_{tot}(CH) - E_{tot}(G) - \sum_i n_i \mu_i, \tag{1}$$

where $E_{tot}(CH)$ is the total energy of Li on a CH divacancy configuration in a 6×6 graphane supercell and $E_{tot}(G)$ is the total energy of 6×6 pristine graphane. The μ_i in equation 1 represents the chemical potential of H, C and Li atoms calculated as the total energies per atom of isolated hydrogen molecules in a large box, graphene and Li in bulk body centered cube (BCC), respectively. n_i represents the number of atomic species (H, C and Li atoms) removed or adsorbed on the graphane monolayer system.

To assess the interactions between the Li adatoms and various configurations of CH divacancies in graphane monolayer, we calculated the binding energies as follows:

$$E_b = \frac{E_{tot}(CHLi) - E_{tot}(CH) - n_{Li}E_{tot}(Li)}{n_{Li}}, \tag{2}$$

where $E(CHLi)$ is the total energy of Li adatom on a CH divacancy in a 6×6 graphane supercell, $E(CH)$ is the total energy of 6×6 graphane with divacancy and $E(Li)$ is the total energy per adatom of Li in a bulk body centered cube (BCC).

3. Results and Discussion

3.1. Proposed Structures Studied

Firstly, we demonstrate how different CH pair divacancy configurations are identified on an isolated single hexagon in a graphane monolayer. A single hexagon in a graphane monolayer is shown in Figure 1 circled with purple. The numbers 1-6, position around an isolated single hexagon, serve as labels for the CH pairs that should be removed during the vacancies creation in this study. These numbers 1-6 are also used to name different vacancy configurations. In this paper, we report a systematic study of different CH pair divacancy configurations presented in Figure 1.

Three distinct configurations are identified as follows: (1) v_{12} configuration, this configuration consist of a CH divacancy where two CH pairs are adjacent to each other. It is denoted as v_{12} configuration, meaning that two adjacent CH pairs are removed from positions 1 and 2 of the single hexagon, as illustrated in Figure 1. (2) v_{13} divacancy configuration, in this configuration there are two CH pairs vacancies at positions 1 and 3, with which CH pair at position 2 separate them. (3) v_{14} configuration, this configuration represents the two CH pair vacancies at positions 1 and 4, facing each other, and separated by the two CH adjacent pairs. These configurations describe different arrangements of CH pair vacancies within the hexagonal structure.

Preprints (www.preprints.org) | NOT PEER-REVIEWED | Posted: 22 November 2023 doi:10.20944/preprints202311.1395.v1

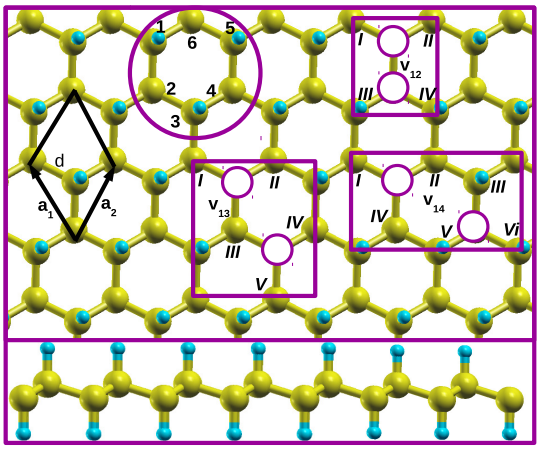

Figure 1. Top panel present top view of the ball-and-stick model of graphane structure, while bottom panel present side views of graphane structure. Different CH pair divacancy configurations v_{12}, v_{13} and v_{14} positions are shown. The white and purple circles hide the numerically labeled CH pair vacancies that are created. The rectangular shapes that enclose vacancy configurations primarily connect the carbon atoms through their potential dangling bonds before undergoing structural relaxation. These carbon atoms are labeled with the roman numbers. The black rhombus shape represents the primitive unit cell of graphane structure, consisting of two C and two H atoms. The vectors $\mathbf{a}_1$ and $\mathbf{a}_2$ correspond to its Bravais lattice vectors. The C and H atoms are represented by the yellow and light blue spheres respectively.

3.2. Thermodynamic Stability and Structural Properties of Different CH Vacancy Configurations

As a common practice in first-principles work, the relative stabilities of various vacancy defects configurations in the host materials are evaluated through the formation energy analysis. In this study, we conduct a comparative analysis of energetic stability of previously mentioned distinct divacancy configurations, namely v_{12}, v_{13} and v_{14}. This comparison is based on their calculated formation energies ($E_{Form}(v)$), as illustrated in Figure 2 and indicated by the red circles. All calculations are computed at the same level of accuracy. As shown in Figure 2a, divacancy configuration v_{12} has the lowest formation energy of 2.71 eV/v_{CH}. This value is 2.21 eV/v_{CH} and 2.00 eV/v_{CH} lower than those of v_{13} and v_{14}, respectively. Perhaps this could be the reason the previous study [24] only report properties of v_{12} divacancy configuration. As is often observed in many material studies, we have observed that the thermodynamic stability of the v_{12}, v_{13} and v_{14} configurations is significantly influenced by the structural reconstruction and the behavior of dangling bonds around the vacancy within a graphane layered structure, after relaxation.

Preprints (www.preprints.org) | NOT PEER-REVIEWED | Posted: 22 November 2023 doi:10.20944/preprints202311.1395.v1

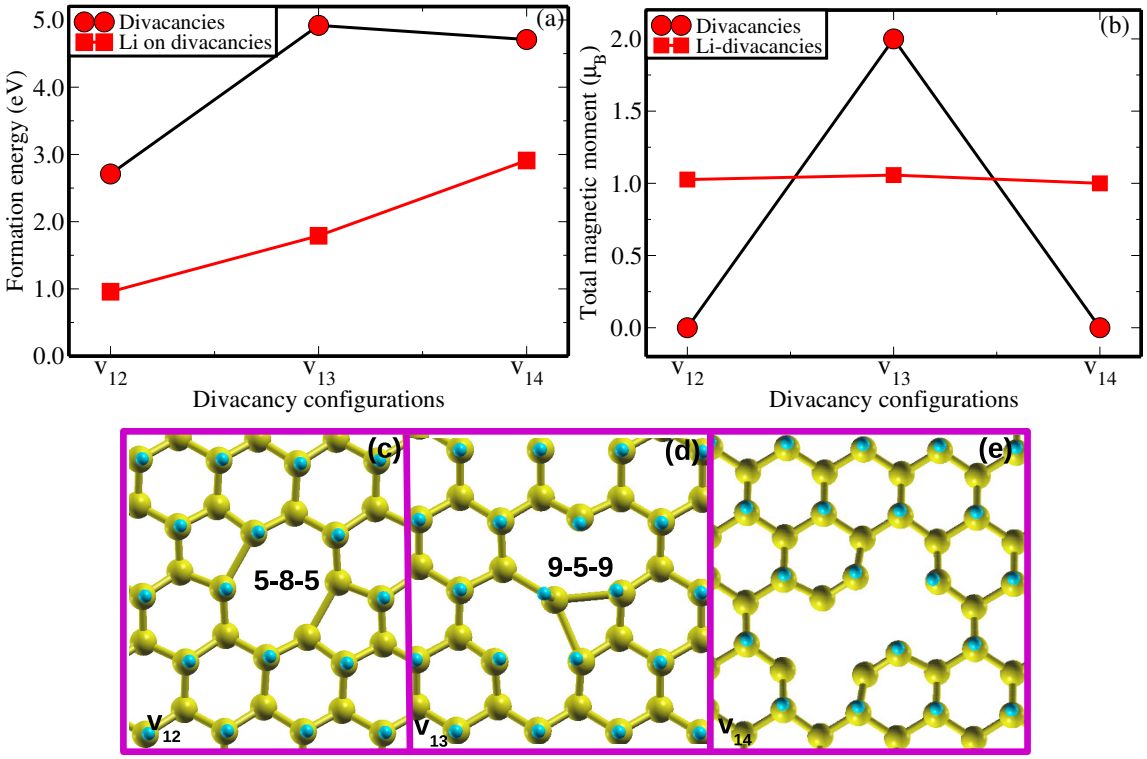

Figure 2. (a) The formation energies of different CH divacancy configurations (v_{12}, v_{13} and v_{14}) are indicated by the circle spheres while those of a Li atom on the different CH divacancy configurations (Li-v_{12}, Li-v_{13} and Li-v_{14}) are represented by the square shapes.(b) The total magnetic moments arising from the v_{12}, v_{13} and v_{14} configurations are indicated by the circle spheres while those influenced by a Li atom adsorption on the different CH divacancy configurations (Li-v_{12}, Li-v_{13} and Li-v_{14}) are represented by the square shapes. (c-e) The relaxed structures of different CH divacancy configurations (v_{12}, v_{13} and v_{14}) created in a 9×9 supercell. Each divacancy configuration reconstructs to form a peculiar type of a topology defect.

In v_{12} configuration (seen in Figure 2c), the pair dangling C atoms I and II as well as the C atoms III and IV attract each other 'to a certain extent' forming a weak bondlength of $d_{I,II} = d_{III,IV} =$ 1.99 Å after geometry optimization. This structural reconstruction or self-healing forms a 'peculiar' vacancy defect type of 5-8-5 divacancy structure as shown in Figure 2c, is in good agreement with the results of Ref [24]. Such type of defect has experimentally been realized in graphene, the mother of graphane, using the high-energy ion beams creating a stable carbon chain [30]. Figure 2b shows that v_{12} lacks a magnetic moment, indicating that structural reconstruction of the dangling C atoms suppresses any potential magnetic moment in agreement with Ref [24].

In a v_{13} divacancy configuration, a C atom III having possibly two unpaid electrons (based on electronic counting) relaxes towards another two C atoms II and IV. The equivalent bond distances $d_{III,II}$ and $d_{III,IV}$ of 2.42 Å are formed between C atoms III and II as well as between C atoms III and IV, respectively. This reconstruction of v_{13} divacancy configuration yields an unusual defect structure of 9-4-9 type (see Figure 2d). It is possible that the construction of 9-4-9 defect structure does not saturates all the dangling bonds surrounding the vacancy, hence the magnetic moment of 1 μ_B has been achieved (Figure 2b). This could be attributed to the C atoms I and III each still having an unpaired electron after structural relaxation. Figure 2e presents the relaxed geometry of a v_{14} divacancy configuration. The C atoms I, II, III, IV, V and VI are unable to rearrange to form any typical vacancy defect. Based on electron counting, v_{14} remains with six unpaired electrons (one electron on each C atom I, II, III, IV, V and VI) after structural relaxation. The absent of total magnetic moment in this system (Figure 2b) could be the result of the cancellation of opposite electronic spins.

 doi:10.20944/preprints202311.1395.v1

3.3. *Effect of Li on the Energetic Stability and Structural Properties of Different CH Vacancy Configurations*

We now examine the effects of Li atom on the energetic stabilities, structural and electronic properties of v_{12}, v_{13} and v_{14} configurations. Initially, we adsorbed Li atom on the biggest hollow site of each vacancy configuration, i.e v_{12} (octagon site), v_{13} (nanogon site) and v_{14}(largest site). Figure 2a shows the effect of Li atom on the energetic stability of v_{12}, v_{13} and v_{14} configurations. It is noted that the Li atom energetically stabilizes the v_{12}, v_{13} and v_{14} configurations through reduction of their formation energies. The formation energy of Li-v_{12} configuration, which is 0.96 eV, suggests that although it is endothermic (requiring an input of energy), it can be relatively easily synthesized compared to the Li-v_{13} and Li-v_{14} configurations.

Figure 3a–c present the relaxed structures of Li atom on the different CH divacancy configurations Li-v_{12}, Li-v_{13} and Li-v_{14}, respectively. In these configurations, the Li atom relaxes closer to the hollow site, which has an impact on the local vacancy structures. Figure 3(a) shows that in the case of Li-v_{12}, Li atom remains within the octagon hollow site leading to a height of 0.00 Å (insertion to remain in-plane with other C atoms). Consequently, this results in an increase in the bond distances $d_{III,II}$ and $d_{III,IV}$ to 2.63 Å equivalently. This has led to the high amount of the binding force (greater enchoring) between Li and the substrate with a binding energy of 3.25 eV. The Li-v_{12} interactions induced a magnetic moment of 1.00 μ_B as shown in Figure 2b. Figure 3b shows that Li-v_{13} buckled up after relaxation, hence this leads to a height of 0.62 Å with a binding energy of 2.07 eV. Figure 2b shows that Li adsorption on a v_{13} reduces the magnetic moment from 2.00 μ_B to 1.00 μ_B. In this configuration, the vacancy defect structure of 9-4-9 reconstructs to create a penta ring and v_{CH} (closest to each other) separated by a newly formed bondlength $d_{III,II}$ of 1.72 Å. The latter value is less than that of its counterpart in 5-8-5 defect without a Li atom. In the Li-v_{14} configuration, the Li atom relaxes to a height of 1.54 Å with a binding energy of 1.99 eV. Notably, there is no significant reconstruction observed in this configuration, as depicted in Figure 3c.

The binding energies for Li-v_{12}, Li-v_{13} and Li-v_{14} configurations, respectively, are relatively larger than that of Li on pristine graphene (1.04) eV [31] and on a single vacancy (v_{CH}) in graphane [15], calculated on the same level of accuracy. The binding energies between Li and v_{12}, v_{13} and v_{14} configurations are more than the Li bulk cohesive energy (1.63 eV), suggesting no chances of Li clusters formation but possible short time Li charging.

Preprints (www.preprints.org) | NOT PEER-REVIEWED | Posted: 22 November 2023 doi:10.20944/preprints202311.1395.v1

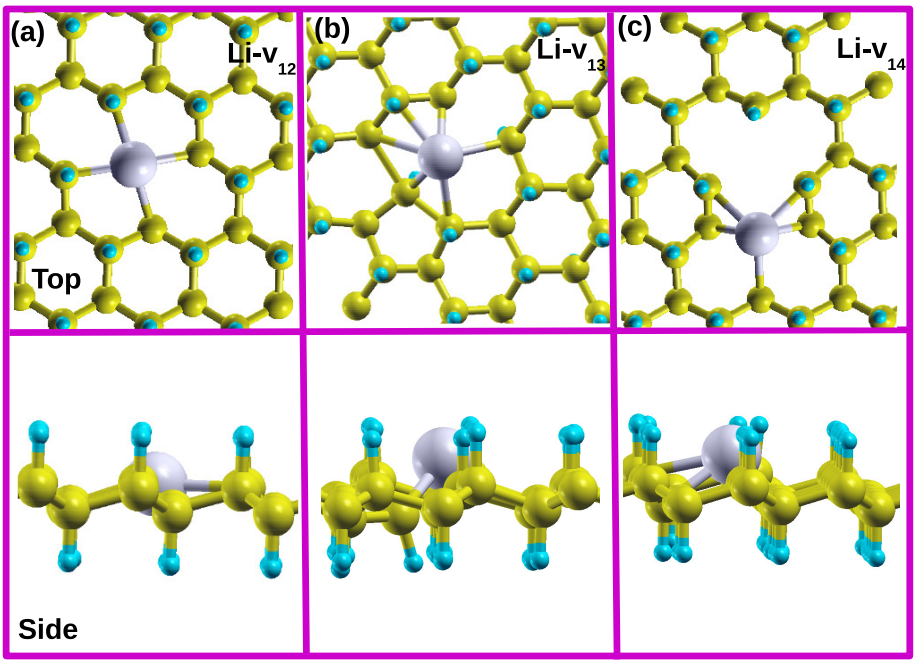

Figure 3. The relaxed structures of Li atom on the different CH divacancy configurations (a) Li-v_{12}, (b) Li-v_{13} and (c) Li-v_{14} created in a 9×9 supercell. In some configurations, Li atom enforces divacancy configuration reconstruction.

3.4. Influence of Different Charge States (-1, and +1) on the Energetic Stability, Structural and Electronic Properties of Li-v_{12}

In this section, we examined the effects of Li charge state alteration on the energetics, local structure around the v_{12} vacancy and electronic properties (DOS) and make camprison with those of the uncharged structure. The charge states considered on Li-v_{12} are q = -1 and +1 of which their respective structures are denoted as Li^{-1}-v_{12} and Li^{+1}-v_{12}. The binding energies for Li^{-1}-v_{12} and Li^{+1}-v_{12} structures are 3.21 eV and 2.24 eV respectively. In comparison with the uncharged binding energy shown in Table 1, the charge doping reduces the binding force between the Li atom and v_{12} substrate, significantly in configuration Li^{+1}-v_{12}.

Table 1. Comparing the binding energies E_b (in eV) and distances between Li atom and graphane d_{Li} (in Å) for Li-v_{12}, Li-v_{13} and Li-v_{14} configurations with that of Li on graphene (Li-*graphene*).

Configurations	E_B	d_{Li}	Vacancy reconstruction
Li-v_{12}	3.25	0.00	5-8-5 changes to divacancy symmetry
Li-v_{13}	2.07	0.62	9-4-9 translates to penta ring and v_{CH}
Li-v_{14}	1.99	1.14	None
Li-v_{CH}	1.72[a]	1.54[a]	None
Li-*graphene*	1.10[b], 1.29[c]	1.71[b] 1.69[c]	None

[a]Ref[15],[b]Ref[31] and [c]Ref[32]

In the case of an addition of electron (Li^{-1}-v_{12}), a Li atom remains within the octagon hollow site, maintaining the same in-plane level with other C atoms leading to a height of 0.00 Å as shown in Figure 4a. Figure 4a shows that the bond distances $d_{III,II}$ and $d_{III,IV}$ increases slightly by 0.03 Å as compared to uncharged Li-v_{12} (Figure 4b), which is an indication that an addition of electron in to the system (Li^{-1}-v_{12}) increases the repulsion force between the C atoms surrounding the Li atom. For the removal of electron (Li^{+1}-v_{12}), Li atoms moves slightly upward to a height of 0.51 Å. Figure 4b shows that the bond distances $d_{III,II}$ and $d_{III,IV}$ decreases significantly by 0.25 Å as compared to uncharged

Preprints (www.preprints.org) | NOT PEER-REVIEWED | Posted: 22 November 2023 doi:10.20944/preprints202311.1395.v1

Li-v_{12} (see Figure 4b). This is an indication that the removal of electron from the system (Li^{+1}-v_{12}) enhances the attraction force between the C atoms surrounding the Li atom.

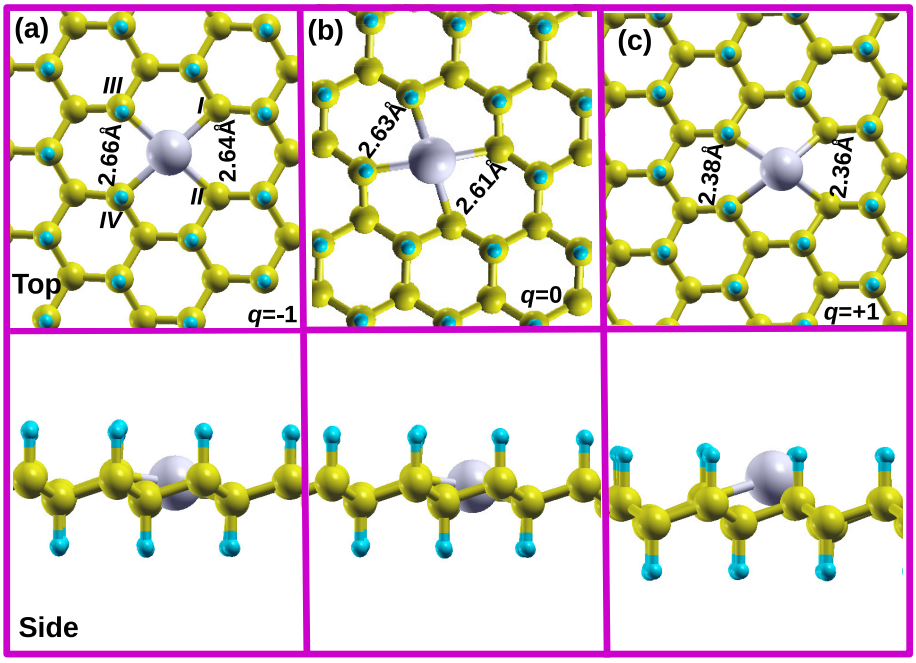

Figure 4. The relaxed structures of Li-v_{12} at different charge states; (a) Li^{-1}-v_{12}, (b) Li^{0}-v_{12} and Li^{+1}-v_{12}.

Figure 5 presents the density of states (DOS) for the most stable Li-v_{12} configuration, comparing with that of without Li counterpart (v_{12}). Figure 5a (top panel) shows that v_{12} has the insulating features with a wide band gap of 4.18 eV (HSE06) between the valence band maximum (VBM) and conduction band minimum (CBM). The VBM and CBM are mainly contributed by the carbon p orbital states as shown on Figure 5a (bottom panel). This is in agreement with Pujari *et al.*[24] reporting that the carbon atoms surrounding the divacancy rearrange to form two new σ bonds leading to the formation of 5-8-5 ringed structure with a band gap of 3.00 eV (GGA). Figure 5b (top panel) shows the effects of Li atoms on the DOS of v_{12}. It is noted that Li atom shifts the Fermi level from the VBM towards the middle of the band gap (suggesting an excess of electrons in the system). It also introduces the occupied and unoccupied states at distinct positions with some crossing the Fermi level in a spin up channel, suggesting metallic character. The observed states are due to hybridization of carbon p orbital and Li s orbital states (Figure 5b (bottom panel)). An addition of electron into the system (Li^{-1}-v_{12}) shifts the Fermi level further towards the CBM Figure 5c. It is interesting to realize that the partially filled mid gap states as shown in Figure 5b becomes fully occupied in Figure 5c. The removal of electron from the system (Li^{+1}-v_{12}) shifts the Fermi level back towards the VBM (Figure 5d). Retaining the metallic character of the system with the partially filled states crossing the Fermi level. Alteration of charge states of Li atom changes the electronic behavior of Li-v_{12} structure. We propose that graphane with Li-v_{12} may serve as a suitable electrode material for LIBs. This suitability arises from the potential enhancement of electronic transmission performance mechanisms facilitated by the newly identified Li states.

Preprints (www.preprints.org) | NOT PEER-REVIEWED | Posted: 22 November 2023 doi:10.20944/preprints202311.1395.v1

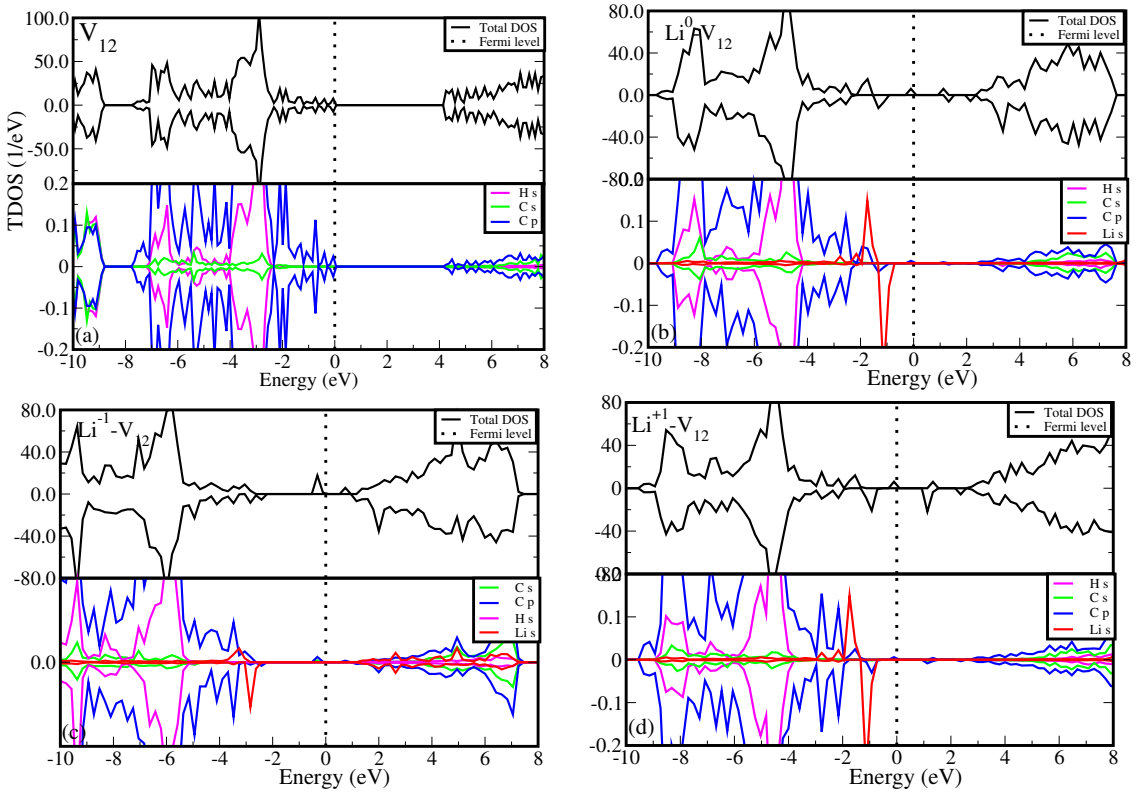

Figure 5. The calculated density of states for (a) v_{12}, (b) Li-v_{12}, (c) Li^{-1}-v_{12} and (d) Li^{+1}-v_{12}. For each sub figure, the top panel represents total density of states, while the bottom panel represents the partial density of states. The Fermi level is set to 0.00 eV and marked by the vertical dashed line.

4. Conclusions

The adsorption mechanisms of Li on graphane with various CH divacancy (v_{12}, v_{13} and v_{14}) configurations have been studied using DFT approach. Firstly, we compared the energetic stability (formation energies) and structural aspects (bond lengths) for v_{12}, v_{13} and v_{14} configurations. Employing structural optimization calculations, it was established that there is a vacancy reconstruction leading to a new defect configuration surrounded by the hexagonal rings in graphane. The v_{12} translated to 5-8-5 defect configuration and is the most stable CH divacancy configuration. Furthermore, we adsorbed Li on v_{12}, v_{13} and v_{14} configurations. The formation energy annalys revealed that Li tends to stabilizes these CH vacancies, with Li-v_{12} being most stable and Li atom relaxes to the same in-plane level with C atoms on the octagon ring. Li interacts strongly with v_{12} at a highest binding energy of 3.25 eV/Li, more than the Li bulk cohesive energy of 1.63 eV/Li. The charge doping Li^{-1}-v_{12} or Li^{+1}-v_{12} alters the energetic stability, structural properties and electronic characters of Li-v_{12}. The Li^{-1}-v_{12} configuration has more binding energy that Li^{+1}-v_{12} configuration. The electronic density of states plot for Li^{-1}-v_{12} reveals an abundance of electrons and increase in conductivity. These interesting observation encourages further studies on designing graphane with vacancies and its characterization for LIBs.

Acknowledgments: The authors acknowledge the University of Pretoria for financial support and availability of computational resources. We express gratitude to the National Institute for Theoretical and Computational Sciences (NITheCS) for funding. Center for high performance computing (CHPC) in cape town is acknowledged for state-of-the-art resources.

References

1. J.M. Tarascon, M. Armand, *Nature* **414** 359 (2001).
2. N. Oyama, T. Tatsuma, T. Sato, T. Sotomura, *Nature* **374** 196 (1995).
3. D.P. Dubal, O. Ayyad, V. Ruiz, P. Gómezromero, *Chem. Soc. Rev.* **44** 1777 (2015).
4. H. Wang, L.F. Cui, Y. Yang, C.H. Sanchez, J.T. Robinson, *J. Am. Chem. Soc.* **132** 13978 (2010).
5. F. Zou, X. Hu, Z. Li, Q. Long, C. Hu, *Adv. Mater.* **26** 6622 (2014).
6. X. Sun, W. Si, X. Liu, J. Deng, L. Xi, *Nano Energy* **9** 168 (2014).
7. K-S. Chen, I. Balla, N. S. Luu, and M. C. Hersam. Emerging opportunities for two- dimensional materials in lithium-ion batteries.*ACS Energy Letters*, **2** (9):2026-2034, (2017). doi: 10.1021/ acsenergylett.7b00476. URL https://doi.org/10.1021/acsenergylett.7b00476.
8. L. Peng, Y. Zhu, D. Chen, R. S. Ruoff, and G. Yu. Two-dimensional materials for beyond- lithium-ion batteries. *Adv. Energ Mater.*, *6* (11):1600025, (2016). doi: https://doi.org/10.1002/aenm. 201600025. URL https://onlinelibrary.wiley.com/doi/abs/10.1002/aenm.201600025.
9. H. Li, Y. Shi, M-H. Chiu, and L-J. Li. Emerging energy applications of two-dimensional layered transition metal dichalcogenides. //doi.org/10.1016/j.nanoen.2015.10.023. *Nano Energy*, **18** :293-305, (2015). ISSN 2211-2855. doi: https: URL https://www.sciencedirect.com/science/article/pii/S2211285515004024.
10. J. O. Sofo, A. S. Chaudhari, and G. D. Barber, *Phys. Rev. B* **75**, 153401 (2007).
11. M.H.F. Sluiter, Y. Kawazoe, Cluster expansion method for adsorption: application to hydrogen chemisorption on graphene.[**?**]hys Rev B **68** 085410 (2003).
12. D. C. Elias, R. R. Nair, T. M. G. Mohiuddin, S. V. Morozov, P. Blake, M. P. Halsall. A. C. Ferrari, D. W Boukhvalov, M. I. Katsnelson, A. K. Geim, and K. S. Novoselov, *Science* **323**, 610 (2009).
13. C. Zhou, S. Chen, J. Lou, J. Wang, Q. Yang, C. Liu, D. Huang and T. Zhu, *Nanoscale Research Letters 9*, 26 (2014).
14. S. Lebègue, M. Klintenberg, O. Eriksson, M. I. Katsnelson., *Phys Rev B* **79** (24), 245117, 1-5 (2009).
15. R.E. Mapasha, M.P. Molepo, N. Chetty, *RSC Adv.* **7**, 63, 39748-39757 (2017).
16. H. Sahin, O. Leenaerts, S. K. Singh, and F. M. Peeters, *Wires Comput. Mol. Sci.* **5**, 255 (2015).
17. E. Keith, Jr. Whitener, *J. Vac. Sci. Technol. A* **36**, 05G401 (2018), https://doi.org/10.1116/1.5034433
18. S. Watcharinyanon, C. Virojanadara, J. Osiecki, A. Zakharov, R. Yakimova, R. Uhrberg, and L. Johansson. Hydrogen interca-lation of graphene grown on 6h-sic(0001), *Surf. Scie.*, **605**:1662-1668, 09 (2011). doi: 10.1016/j.susc.2010.12.018.
19. Y.E. Yang, Y. Xiao, and X.H. Yan. Charge distribution of lithium-doped graphane/graphene hybrid system: Role of nearly-free electronic states. *Sol. Stat. Commun.*, **229**:43-48, (2016). ISSN 0038-1098. doi: https://doi.org/10.1016/j.ssc.2015.12.011. URL https://www.sciencedirect.com/science/article/pii/S0038109815004366.
20. Sahin H, Ataca C, Ciraci S. Electronic and magnetic properties of graphane nanoribbons. *Phys Rev B*, **81**:205417 (2010).
21. H. Sahin, C. Ataca, and S. Ciraci, Magnetization of graphane by dehydrogenation. *Appl. Phys. Lett.* **95**, 222510 (2009).
22. J. Berashevich, and T. Chakraborty, Sustained ferromagnetism induced by H-vacancies in graphane. *Nanotechnology* **21**: 355201 (2010).
23. R E Mapasha, M P Molepo and N Chetty, *Phys. E.* **79**, 52-58 (2016).
24. B. S. Pujari and D.G. Kanhere, *J. Phys. Chem. C* **113**, 21063 (2009).
25. G. Kresse and J. Hafner, *Phys. Rev. B* **47**, 558 (1993).
26. J. Heyd, G. E. Scuseria, and M. Ernzerhof, *J. Chem. Phys.* **118**, 8207 (2003); **124**, 219906 (2006).
27. P. E. Blochl, *Phys. Rev. B* **50**, 17953 (1994).
28. H. J. Monkhorst and J. D. Pack 1976, *Phys. Rev. B* **13**, 5188.
29. S. B. Zhang and J. E. Northrup, *Phys. Rev. Lett.* **67**, 2339 (1991.)
30. Jin C, Lan H, Peng L, Suenaga K, Iijima S. Phys Rev Lett, **102** 205501 (2009).

 doi:10.20944/preprints202311.1395.v1

31. K.T. Chan, J.B. Neaton, M.L. Cohen, Phys. Rev. 77 (2008) 235430.
32. A. M. Garay-Tapia, A. H. Romero, V. Barone, J. Chem. Theory Comput. 8, 3, 1064-1071,(2012)